RESEARCH ARTICLE

INTERNATIONAL RESEARCH JOURNAL OF MULTIDISCIPLINARY TECHNOVATION

Asian Research Association

DOI: 10.54392/irjmt2451

Synthesis and Ionic Conductivity of Lanthanum-based Ceria $Ce_{1-x}La_xO_{2-\delta}$ Electrolytes for Solid Oxide Fuel Cell Applications

S. Seema [a], T. Thangesh [a], T.R. Rajasekaran [a, b], S. Nagarajan [c], V. Sabarinathan [a, b, *]

[a] Department of Renewable Energy Science, Manonmaniam Sundaranar University, Tirunelveli-627012, Tamil Nadu, India
[b] Department of Physics, Manonmaniam Sundaranar University, Tirunelveli-627012, India, Tamil Nadu, India.
[c] Department of Chemistry, Manonmaniam Sundaranar University, Tirunelveli-627012, Tamil Nadu, India
* Corresponding Author Email: sabarinathan.msu@gmail.com

DOI: https://doi.org/10.54392/irjmt2451
Received: 17-05-2024; Revised: 24-07-2024; Accepted: 02-08-2024; Published: 11-08-2024

Abstract: In advanced low temperature solid oxide fuel cell (LT-SOFC) technology, we present a comprehensive study on the effects of lanthanum co-substitution in ceria electrolyte. Using a co-precipitation synthesis approach, we successfully incorporated trivalent La ions into the ceria matrix to improve its structural and functional properties. This study investigates La^{3+} doped CeO_2 solid electrolytes (LDC) synthesis and characterization at varying concentrations (0.2, 0.3, 0.4, and 0.5). The materials were characterized using a suite of analytical techniques. X-ray diffraction (XRD) analysis revealed that all samples maintained a cubic fluorite-type structure with evident changes in peak intensity and broadening as La^{3+} ion concentration increased, indicative of induced lattice defects FT-IR spectra indicated minor modifications in the Ce-O bond vibrational modes. Optical studies demonstrated enhanced absorption in the UV region and a consistent band gap of 3.15 eV across all samples, underscoring the doping's influence on electronic transitions. Scanning electron microscopy (SEM) images highlighted increased grain sizes and improved interparticle connectivity, which is essential for material performance. X-ray fluorescence spectroscopy verified the existence of cerium and lanthanum, proving the successful addition of dopants. Raman spectroscopy also confirmed changes in the structure, indicating alterations in the characteristic vibrational frequencies and a decrease in their intensity as the dopant concentration increased. The conductivity of the material was tested at low temperatures ranging from 573 K to 873 K for use in Solid Oxide Fuel Cells, with the highest conductivity recorded at 0.21 mS/cm at 873 K.

Keywords: Solid Oxide Fuel Cell, Solid Electrolyte, La-Doped Ceo_2, Impedance, Ionic Conductivity, Band Gap, Activation Energy

1. Introduction

The global energy landscape demands highly efficient and environmentally friendly energy sources. Solid oxide fuel cells (SOFCs) are desirable among emerging technologies because they can provide sustainable and efficient electrical energy [1]. In the architecture of SOFCs, electrolytes are important in affecting the overall cell performance. The search for an ideal electrolyte is characterized by high sintering temperatures, manufacturing costs, and suboptimal ionic conductivity, hindering large-scale commercialization [2, 3]. Solid oxide fuel cells (SOFCs) are prominent version devices due to their attractive properties, such as excellent efficiency, low emissions, and fuel flexibility[4-6]. Yttrium-stabilized zirconia (YSZ) is one of the most commonly used electrolytes in SOFCs due to its high ionic conductivity and stability in reducing and oxidizing atmospheres[7, 8]. However, its high operating temperature range of 800-1000 °C is limited. For example, it blocks the movement of ions at the cathode-electrolyte interface by creating an insulating phase in Lanthanum and strontium-based cathodes [9]. Scandia-stabilized zirconia has shown good electrical conductivity, but at high temperatures (Yb_2O_3, Bi_2O_3, Al_2O_3, or Ga_2O_3 with ScSZ [10-15] and also at low temperatures (10 mol %). Therefore, this has raised the interest and need for developing new promising electrolyte materials for low-temperature SOFCs (LT-SOFCs).Along with Salt-Oxide Composites and Nanocomposites for Advanced Fuel Cells [16, 17]. The well-known solid electrolyte material MO_2 (M = Zr, Ce) is still a good candidate for SOFCs [18]. Doped ceria exhibits good ionic conductivity compared to stabilized zirconia by creating oxygen vacancies through which oxygen ions can easily pass [19-23]. Ceria doping/co-doping is a superior path to enhance ionic oxide conductivity by structural modification of CeO_2 [24]. However, ceria-based electrolytes also have drawbacks. The reduction of Ce^{4+} to Ce^{3+}, which at low oxygen

partial pressures (<10-10atm), increases the electronic conductivity [25]. Therefore, many researchers have reported the use of various rare earth transition elements and metal ions, such as Er^{3+}, Dy^{3+}, La^{3+}, Sm^{3+}, Eu^{3+}, Nd^{3+}, $Gd^{3+,}$ Y^{3+}, Ca^{2+} and Sr^{2+} to improve the ionic conductivity of ceria-based electrolytes [26-29]. The ionic conductivity enhancement in doped ceria is due to increased oxygen vacancies. However, these vacancies are not free but rather bound to the doping cations, which may result from defective binding or clustering of oxygen vacancies after reaching the maximum doping concentration [30]. Ionic conductivity is also influenced by the dopant ionic radius and valence. Compatibility of the ionic radius of the host cation (Ce^{4+}) and the dopant is important to obtain a desirable lattice voltage. Otherwise, the mismatch of the dopants tends to introduce a large lattice voltage, reducing the ionic conductivity. In addition, the binding energy of the dopant lattice must be low to allow for an increase in oxygen vacancies [31]. In addition, ceria-based electrolytes have poor mechanical strength. They may be subjected to mechanical and thermal stresses during cell fabrication and high-temperature operation, limiting their realization in practical applications [32, 33]. Therefore, the mechanical strength of ceria can be easily improved by adding rare earth oxides, as the increase in oxygen vacancies contributes to weakening the bond energy, increasing the thermal expansion coefficient (TEC) of ceria [34]. Therefore, the TEC of SOFC components should be matched to prevent cracking during thermal cycling, which improves the stability of SOFCs in transient operation [35, 36]. To date, materials studied as electrolytes for SOFCs have not achieved the desired high ionic conductivity of 0.1 S cm^{-1} at temperatures below 600 °C. Large ionic conductivities and challenges exist in developing new versatile, cost-effective, and stable electrolyte materials suitable for SOFC operation at low temperatures. Cerium oxide doped with alkaline earth and rare earth metals has proven to be an alternative to the more expensive GDC/SDC. It exhibits significant ionic conductivity even at low temperatures, making it suitable for SOFC applications. For example, $Sr_{0.1}Sm_{0.1}Ce_{0.8}O_{2-\delta}$ has been reported to have an ionic conductivity of 0.5 Scm^{-1} at 600°C [37]. Co-doping with alkaline earth metals also reduces the sintering temperature, potentially reducing the operating costs of SOFCs. Recent studies have investigated various compositions of inexpensive La-doped ceria materials as SOFC electrolytes, with favourable results compared to conventional GDC/SDC materials [38]. It can be strongly speculated that the co-doping of alkaline earth metals and La-doped ceria meets the required criteria. In a detailed study, Jaiswal et al. [39] used calcium and strontium co-doped cerium oxide and measured the ionic conductivity value of $Ce_{0.92}Ca_{0.05}Sr_{0.03}O_{1.92}$, which was about 1.22 × 10^{-2} Scm^{-1} at 600°C. In another study, Zheng Y. *et al*. [27] investigated Lanthanum and calcium co-doped ceria-based materials as electrolytes for IT-SOFCs. They found an exemplary ionic conductivity of 3.56 × 10^{-2} S cm^{-1} at 700°C for $Ce_{0.85}La_{0.10}Ca_{0.05}O_{2-\delta}$ evaluated. Regarding low-temperature SOFCs, Ali A. *et al.* [37] comprehensively analyzed various alkaline earth metals, including barium, calcium, magnesium, strontium and doped samarium. Their results showed an impressive ionic conductivity of 0.126 S cm^{-1} with a relatively low activation energy of 0.48 eV and a maximum power density of 630 mW cm^{-2} for the composition $Ca_{0.1}Sm_{0.1}Ce_{0.8}O_{2-\delta}$ for an operating temperature about 600 °C. Momin *et al.* [40, 41] dealt with the synthesis of Lanthanum and calcium-doped ceria of different compositions by combustion and solid-state reaction methods, respectively. The obtained materials showed ionic conductivities of 8.89 × 10^{-3} S cm^{-1} for $La_{0.1}Ce_{0.9}O_{2-\delta}$ [41] and 8.01 × 10^{-3} Scm^{-1} for $Ca_{0.1}Ce_{0.9}O_{2-\delta}$ at 700°C [40]. Lanthanum (La) and alkaline earth metal co-doped ceria systems are exciting due to the smaller band gap and improved ionic mobility. Despite promising results, the literature has no systematic study of different La-Co doping ratios. Hence, there is great interest in studying these materials more comprehensively. The current work centres on advancing lanthanum-doped ceria electrolytes to consider their structural and electrochemical properties. For this reason, $La_{1-x}Ce_xO_{2-\delta}$ [x = 0.2, 0.3, 0.4 & 0.5] (LDC) were synthesized utilizing the co-precipitation strategy in LT-SOFCs. The morphology and structure of these nanocomposite electrolytes were examined utilizing X-ray diffraction (XRD) and filtering electron microscopy (SEM). Electrical conductivity was measured utilizing a four-probe method within the temperature range 873K in the discussion, and electrochemical impedance examination (EIS) was considered on these ceria electrolytes.

2. Materials and Methods

Preparation of Ceria doped lanthanum solid electrolyte materials were prepared using the analytical grade of Cerium (III) nitrate hexahydrate (Sigma Aldrich), Lanthanum (III) nitrate hexahydrate(Sigma Aldrich), sodium carbonate(Sigma Aldrich). The nanocomposites of LDC solid electrolytes were synthesized via the cost-effective co-precipitation method at room temperature with a molar ratio of $Ce_{0.8}La_{0.2}O_2$, $Ce_{0.7}La_{0.3}O_2$, $Ce_{0.6}La_{0.4}O_2$ and $Ce_{0.5}La_{0.5}O_2$ in 200 mL of deionized water and stirred at 250 rpm at 80°C. The preparation method is displayed in Figure 1. The sodium carbonate (precipitating agent) solution was added dropwise to the LDC solution under vigorous stirring. The mixture was allowed to settle for precipitation. The precipitated LDC was dried at 120°C followed by sintering at 800°C for 6 h. The sintered powder was crushed and grinding to obtain homogeneity. The synthesized solid electrolytes were characterized by powder X-ray diffraction (XRD) using Bruker D8 Advance with CuKα radiations (λ = 1.5406 Å).

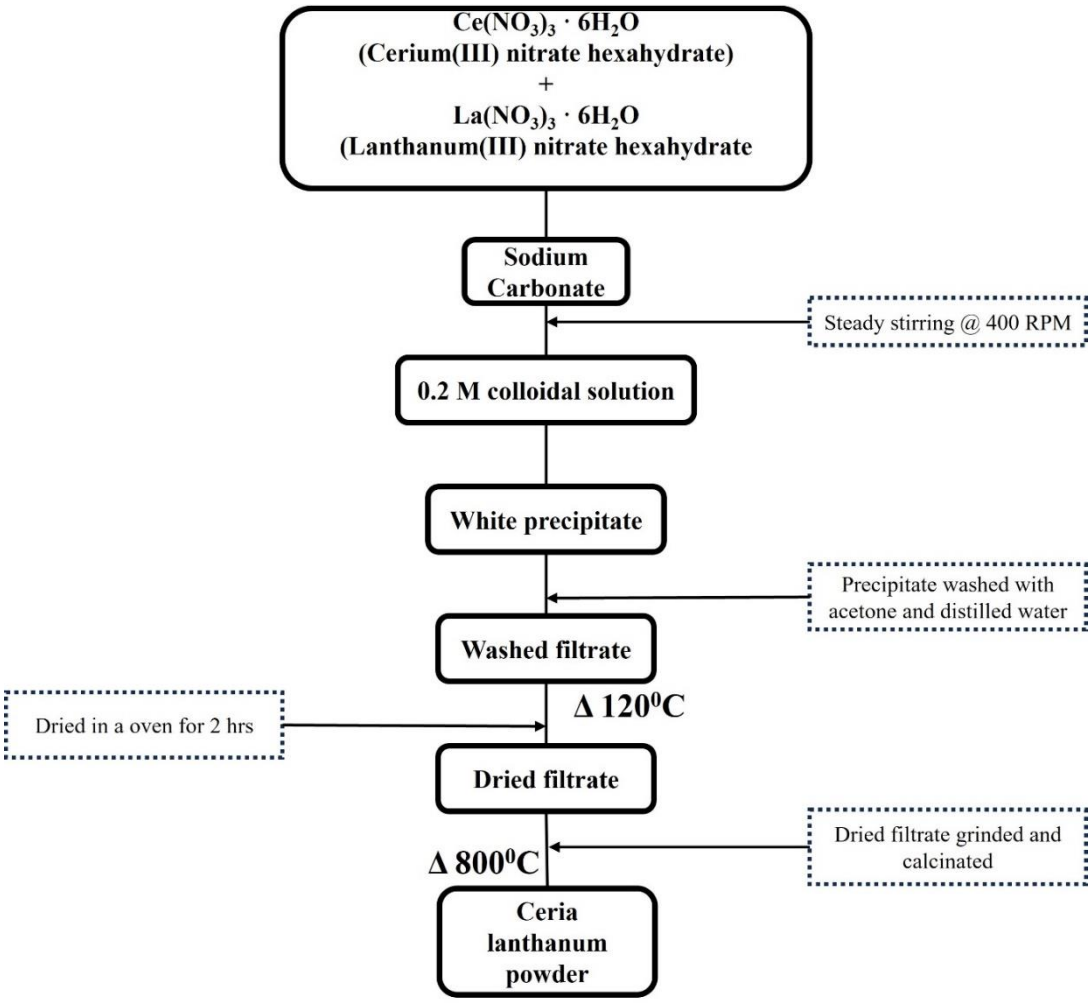

Figure 1. Flow chart of preparation of LDC solid electrolyte

Fourier transform infrared (FTIR) spectroscopy was recorded at a spectral range of 1750 to 550 cm^{-1} using PerkinElmer. The diffuse reflectance spectra were recorded using a PerkinElmer Lambda 35 spectrophotometer. The electrical conductivity was measured using a Biologic electrochemical workstation (Biologic VSP300) with a temperature range of 303 K and 873 K, with a relative density of approximately 95%. As prepared, LDC samples were pelletized using an 8mm diameter under a hydraulic press with a pressure of 7 tons for 5 min. Then, all the pellets were sintered at 800° C for further characterization. The structural and vibrational studies of LDC solid electrolytes were conducted using Raman spectroscopy with a spectral range of 50 to 1000 cm^{-1} on the WITEC ALPHA 300-R instrument with a source wavelength of 532 nm. The morphology of the electrolyte samples was examined using SEM with the TESCAN VEGA3 LMU instrument.

3. Results and Discussion

3.1 Phase Analysis

The XRD pattern is a powerful tool for elucidating the crystalline Nature and structural characteristics of the La^{3+} doped CeO_2 samples. Figure 2 displays the X-ray Diffraction (XRD) pattern collected from examining different levels of La^{3+} ions added to the CeO_2 system. Each sample showed a clear, crystalline structure with a cubic fluorite-like arrangement (JCPDS Card No: 65-2975) [42]. It's clear that as the amount of La^{3+} ions increased, the strength of each reflection peak decreased, along with the peaks becoming wider. Moreover, additional reflection peaks were observed. The (111), (220), and (311) reflection peaks were noted to separate into pairs and then triplets. This behavior can be explained by the higher concentration of dopants, which mainly leads to the formation of interstitial planes and defects instead of filling in the substitution spots in the CeO system [43].

Across all concentrations, the XRD patterns depict a well-defined crystalline structure consistent with the cubic fluorite-type structure. This observation underscores the robust crystallinity of the CeO_2 system, even upon doping with La^{3+} ions. A notable trend from the XRD patterns is the peak intensity and broadening with increasing La^{3+} ion concentration. Specifically, as the concentration of La^{3+} ions increases, a gradual decrease in the intensity of all reflection peaks is observed, accompanied by broadening effects.

Ultimately, the lattice parameter estimated for all samples is 5.3693 Å, and the crystallite size is 34.38 nm using the Scherrer formula. This phenomenon suggests changes in the crystallite size and lattice strain induced by doping.

Furthermore, secondary reflection peaks emerge with increased La^{3+} ion concentration [49]. On the minimum concentration of La^{3+}, the ions are overlapped. Further increase of La^{3+} concentration indicated its presence by secondary peaks, confirmed by pure lanthanum ions JCPDS card no – 36-1481. Particularly noteworthy is the observation that primary reflection peaks, such as (111), (220) and (311), undergo splitting into doublets and, subsequently, triplets. This splitting phenomenon is indicative of structural modifications induced by the doping mechanism.

The splitting of reflection peaks into multiple components can be attributed to the increasing dopant concentration, which primarily fosters the creation of interstitial planes and defects within the CeO_2 lattice rather than occupying substitutional positions [44]. This propensity for defect formation becomes more pronounced as the La^{3+} ion concentration escalates, leading to the observed structural alterations manifested in the XRD patterns. Here, composition x = 0.3 shows a slight difference in its peak, possibly due to its lattice defect or materials impurities. Therefore, further characterizations are done for the other compositions, excluding x = 0.3.

3.2 FTIR Studies

Figure 3 presents the FTIR spectra of CeO_2 electrolyte samples doped with varying concentrations of La3+ ions (0.2, 0.4, and 0.5), recorded between 4000 and 400 cm^{-1}. Notable peaks at 523 and 547 cm^{-1} correspond to the F_{2g} mode of the ceria cubic lattice, indicating that the cubic structure is maintained despite doping [45]. Additionally, weak bands at 1064, 1121, and 1194 cm^{-1} are associated with the stretching vibrational modes of Ce-O bonds and higher-order modes, respectively, suggesting that La^{3+} doping induces subtle changes in the lattice dynamics [44-48]. These observations confirm the structural stability of the doped ceria and provide insights into modifications in its vibrational characteristics, crucial for optimizing its performance as an electrolyte in applications like solid oxide fuel cells.

3.3 Optical Studies

Figure 4a presents the optical absorption spectra of CeO_2 electrolyte samples doped with varying concentrations of La^{3+} ions (0.2, 0.4, & 0.5), recorded between 200 and 800 nm. All samples show broad and strong absorption in the ultraviolet (UV) region, attributed to charge transfer between O^{2-} (2p) and Ce^{4+} (4f), with weaker absorbance in the visible region [46]. As the La^{3+} doping concentration increases, there is a slight increase in absorbance in the visible region and a corresponding decrease in the UV region.

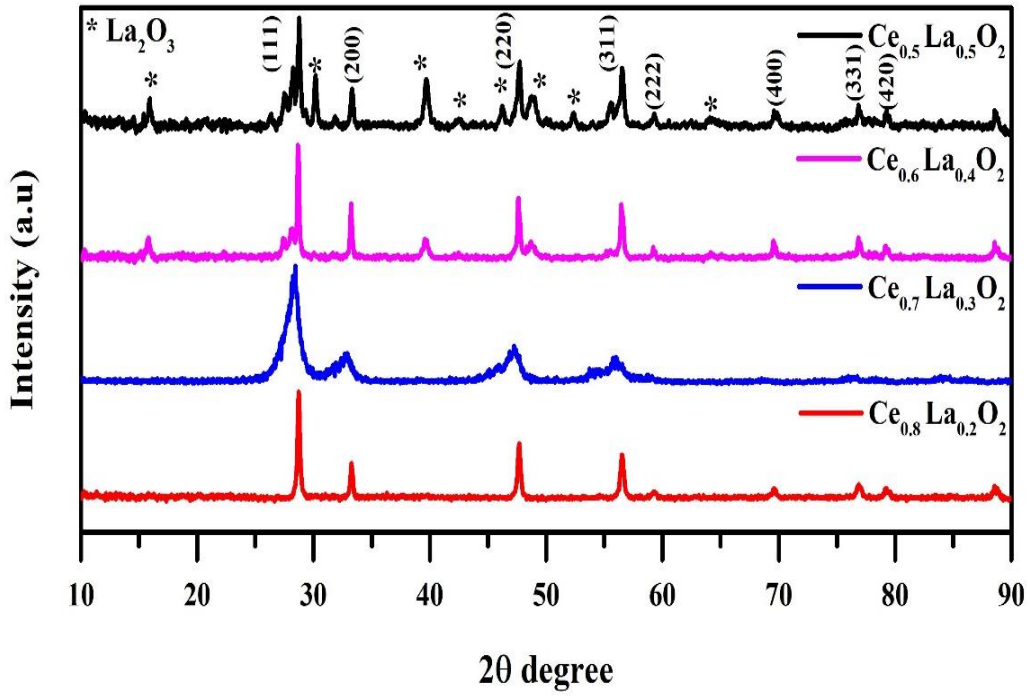

Figure 2. XRD pattern of Ce1−xLaxO2−δ concentrations of x = 0.2, 0.4, 0.5 LDC solid electrolyte.

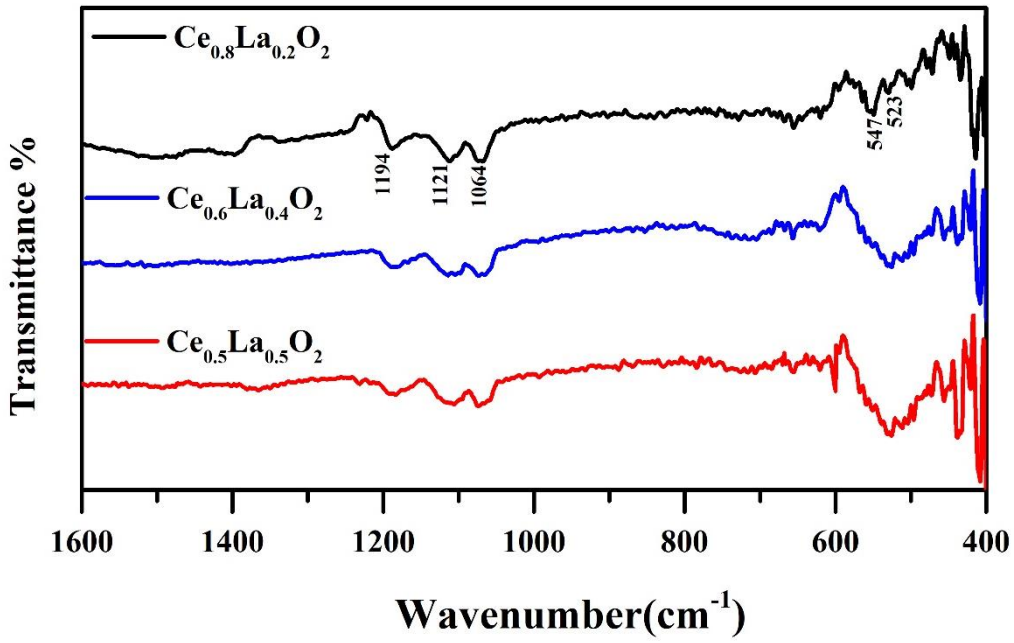

Figure 3. FTIR spectra of Ce1−xLaxO2−δ concentrations of x = 0.2, 0.4, 0.5 LDC solid electrolyte.

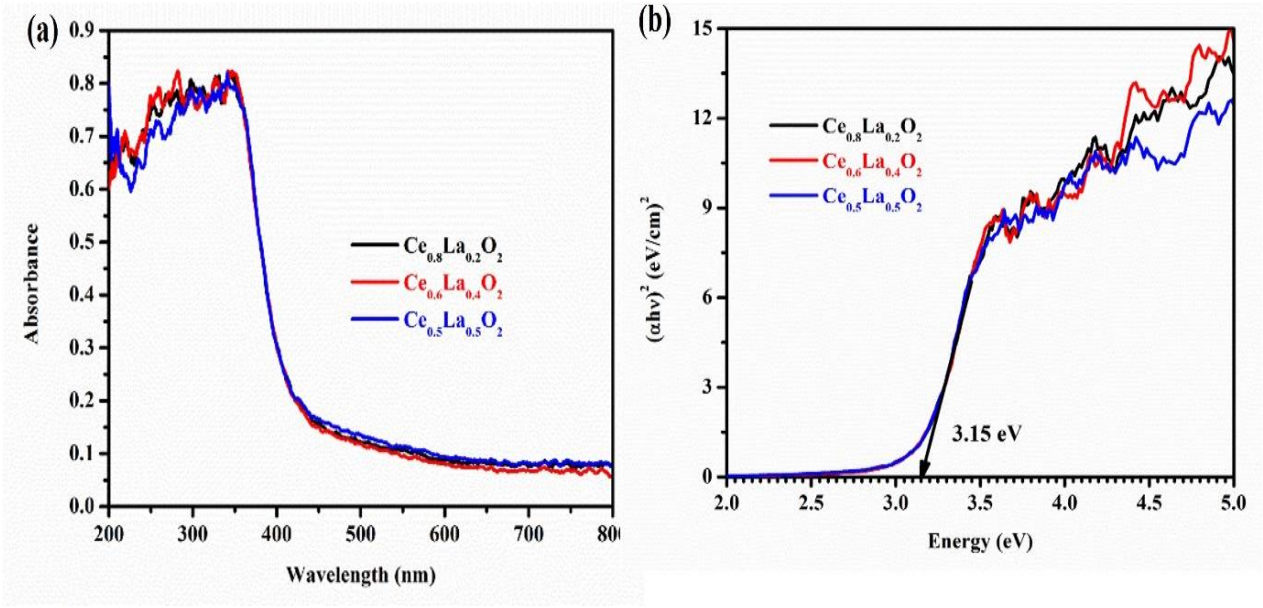

Figure 4. (a) Optical Absorbance spectra (b) The band gap value of $Ce_{1-x}La_xO_{2-\delta}$ concentrations of x = 0.2, 0.4, 0.5 LDC solid electrolyte

This trend suggests that La^{3+} ions modify the electronic structure of CeO_2, enhancing its visible light absorption while reducing UV absorbance, potentially altering the material's optical properties for various applications. Figure 4b displays the energy band gap values for CeO_2 electrolyte samples doped with different concentrations of La^{3+} (0.2, 0.4, & 0.5) ions. From the absorption spectra, the band gap energy (Eg) of the solid CeO_2 electrolytes was calculated using Tauc's equation,

$$\alpha h\upsilon = A(h\upsilon - E_g)^n \qquad (1)$$

where A is a constant value, hυ is the photonic energy, n is a constant which depends on the probability of transition, and α is the absorption coefficient. CeO_2 is a direct band transition material, and hence n = 2. Plotting $(\alpha h\upsilon)^2$ as a function of photon energy and extrapolating the linear portion of the curve to absorption equal to zero, as shown in Fig. 4b, gives the direct band gap values of La^{3+} doped CeO_2 electrolyte. The bandgap value was calculated to be 3.15 eV for all samples. Interestingly, the dopant does not seem to affect the lattice of the CeO_2 electrolyte, as corroborated by XRD analysis. It is confirmed that La^{3+} dopant ions did not replace the Ce^{4+} ions; however, they introduce new planes within the CeO_2 crystal structure. Our result agrees with the previously reported band gap (Eg) values [47].

3.4 Morphological Analysis

The SEM and EDAX analyses conducted in this study provide a detailed examination of the morphology and elemental composition of the materials for CeO_2 electrolyte samples doped with different concentrations of La^{3+} (0.2, 0.4, & 0.5) ions, as illustrated in Figure 5 (a, b, c) and (d, e, f), respectively. The morphology of La^{3+}-doped CeO_2 samples with varying concentrations (in Figures (a,c,e) reveals several critical features that highlight enhanced interparticle connectivity. This connectivity significantly contributes to the overall structure, resulting in an agglomerated and porous framework, which is crucial as it influences the material's physical and chemical properties.

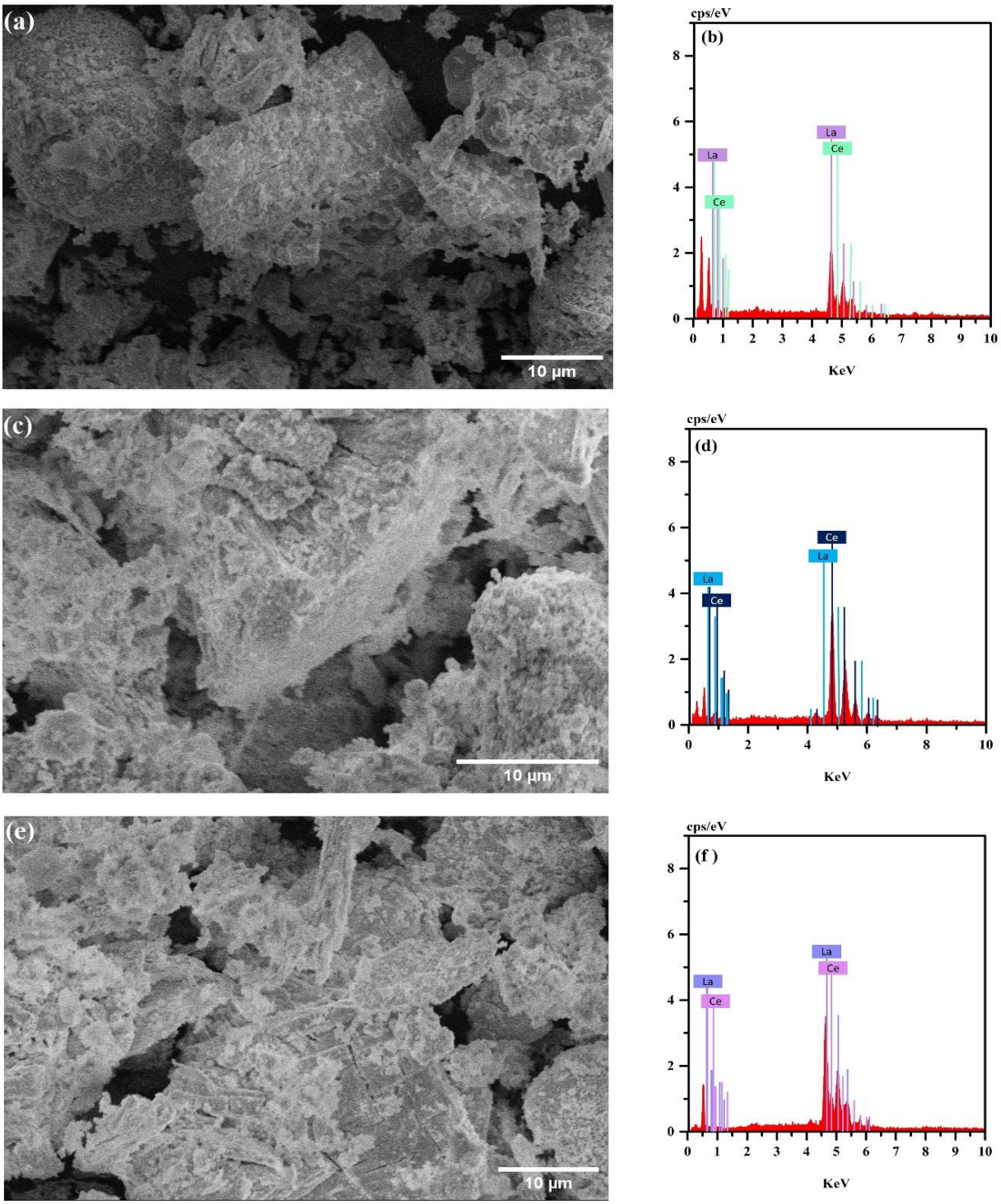

Figure 5. (a, b), (b, c), (d, e) were the respective SEM and EDAX image for $Ce_{1-x}La_xO_{2-\delta}$ concentrations of x = 0.2,0.4,0.5 LDC solid electrolyte

Upon closer examination, the SEM images display larger grain sizes across the samples. This grain size increase can be attributed to the formation of larger clusters, driven by the substantial surface area provided by the smaller crystallites. Particles with smaller crystals typically have a higher ratio of surface area to volume, which makes it easier for them to form bigger clumps as they interact and stick together more effectively. The structure seen through scanning electron microscopy (SEM) clearly reveals a more uniform spread of particle sizes in the material's porous structure. This even distribution of particle sizes is key, leading to more stable and predictable properties of the material, which is important for a variety of uses like catalysis, sensor development, and energy storage technologies. Moreover, the shape of the particles' surfaces is shown to be closely packed. This dense arrangement is not just a structural aspect but also plays a crucial role in the material's performance. In particular, a closely packed surface shape improves the ability to separate charge carriers. The ability to efficiently separate charge carriers is beneficial in many areas, especially in solar cells and photocatalysts. To sum up, the SEM images offer a detailed look into the microscopic structure of the samples. The increased connection between particles, the formation of larger grains due to more cluster formation, the narrower spread of particle sizes, and the tightly packed surface shape all contribute to the material's enhanced properties and potential advantages in various applications. The EDAX spectra, depicted as (b), (d), and (e), provide essential information on the elemental makeup of the samples being studied. Specifically, clear peaks in these spectra confirm the dominance of Cerium and Lanthanum in the samples under investigation. In conclusion, the EDAX spectra act as succinct yet informative tools for determining the main elemental composition of the samples, underscoring the high presence of Cerium and Lanthanum in the studied materials.

3.5 Raman Spectra

Figure 6 displays a Raman spectroscopy analysis that offers detailed insights into the structural behaviors of CeO_2 electrolyte samples, each differing in the amount of La^{3+} ions (0.2, 0.4, & 0.5 M) they contain. The data, spanning from 50 to 1000 cm^{-1}, gives a thorough perspective on how these materials vibrate. A significant observation from the Raman spectra is the prominent Raman-active vibration peak at 455 cm^{-1} present across all samples. This peak points to the F2g vibration mode of the ceria cubic lattice, indicating the symmetrical behavior of oxygen ions around each Ce^{4+} cation, which is a key feature of the cerium oxide structure as shown in references 3, 4, and 5. As the amount of La^{3+} ions increases, there's a notable decrease in the amplitude of the F2g vibration, indicating the La^{3+} doping effect. This decrease in amplitude is due to the La^{3+} ions creating additional lattice planes, which disrupt the original symmetry, thus reducing the F2g mode's intensity. Furthermore, as La^{3+} concentration rises, there's a slight shift in the position of the F2g mode peak, indicating changes in the lattice's parameters and the surrounding environment around Ce^{4+} cations, supporting the idea that La^{3+} has a significant impact on the structural characteristics of CeO_2 electrolytes. In conclusion, this analysis effectively highlights how the addition of La^{3+} ions changes the vibrational behavior and lattice structure of CeO_2 electrolytes, providing crucial insights on the effects of doping on these materials.

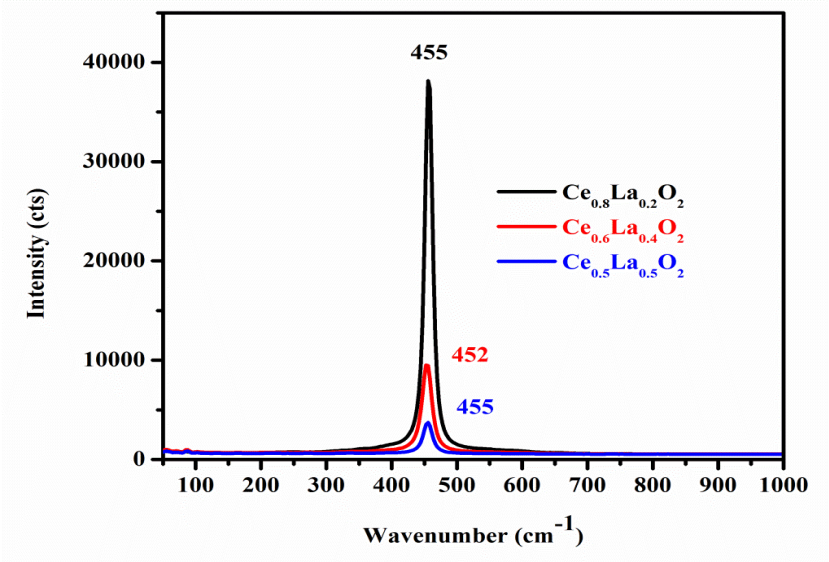

Figure 6. Raman Spectra of $Ce_{1-x}La_xO_{2-\delta}$ concentrations of x = 0.2, 0.4, 0.5 LDC solid electrolyte.

3.6 Electrochemical Studies

Potential electrochemical impedance spectroscopy data were measured using a VSP-300 biologic multichannel potentiostat. The Electrochemical impedance (EIS) spectra were measured between a frequency window of 100 MHz to 7 MHz with a sinus amplitude V_a = 50 mV. Nyquist impedance data of prepared solid electrolytes named $Ce_{0.5}La_{0.5}O_2$, $Ce_{0.6}La_{0.4}O_2$ and $Ce_{0.7}La_{0.3}O_2$, $Ce_{0.8}La_{0.2}O_2$ were measured with the same setup. Nyquist plots of $Ce_{0.5}La_{0.5}O_2$, $Ce_{0.6}La_{0.4}O_2$, $Ce_{0.7}La_{0.3}O_2$, and $Ce_{0.8}La_{0.2}O_2$ were shown in figure 7(a) and 7(b) respectively. EIS spectra were fitted using an equivalent circuit of R1+CPE1/R2+CPE2 to determine solid electrolytes grain and grain boundary response. R1 and R2 were resistance associated with grain and grain boundary response. Whereas, CPE the constant phase element accounts to the capacitance behaviour. Resistance R1 and Constant phase element CPE1 are in series connection parallel to the Resistance R2 which is in series connection with Constant phase element CPE2. The total resistance Rt was determined from the grain and grain boundary resistance. The electrical conductivity of solid electrolytes was calculated from the expression of $\sigma = \frac{L}{R_t A}$, where L, A and R_t are the thickness, cross-sectional area and total resistance of solid electrolytes, respectively[47]. Conductivity (σ) of $Ce_{0.5}La_{0.5}O_2$, $Ce_{0.6}La_{0.4}O_2$ and $Ce_{0.7}La_{0.3}O_2$, $Ce_{0.8}La_{0.2}O_2$ was 1.95×10^{-2} Scm^{-1}, 1.56×10^{-2} Scm^{-1}, 1.54×10^{-2} Scm^{-1} and 1.53×10^{-2} Scm^{-1} respectively at room temperature shown in table 1. Maximum conductivity of $\sigma = 1.53\times10^{-3}$ Scm^{-1} was observed for $Ce_{0.8}La_{0.2}O_2$; subsequently, an increase in dopant x = 0.3, 0.4 and 0.5 of La have a negative impact on conductivity (σ) as tends to decrease as the dopant concentration increase as in figure 7. Boaro et al. reported 8.40×10^{-2} Scm^{-1} at 1000^0C for $Ce_{0.8}Zr_{0.2}O_2$ [48]. Amar et al reported $Ce_{0.8}Zr_{0.2}O_{1.9}$ ($\sigma = 0.198\times10^{-3}$ Scm^{-1}), $Ce_{0.7}Zr_{0.3}O_{1.85}$ ($\sigma = 0.208\times10^{-3}$ Scm^{-1}), $Ce_{0.6}Zr_{0.4}O_{1.8}$ ($\sigma = 0.745\times10^{-3}$ Scm^{-1}) at 600^0C [49]. Conductivity studies on room temperature for $Ce_{1-x}La_xO_{2-\delta}$ concentrations of x = 0.2,0.4,0.5 LDC electrolyte reveals lower La concentration offers better electrical conductivity listed in table 1.

Table1. Conductivity of Lanthanum doped ceria at room temperature

Electrolyte	Conductivity ($mScm^{-1}$)
$Ce_{0.8}La_{0.2}O_2$	1.53×10^{-2}
$Ce_{0.7}La_{0.3}O_2$	1.54×10^{-2}
$Ce_{0.6}La_{0.4}O_2$	1.56×10^{-2}
$Ce_{0.5}La_{0.5}O_2$	1.95×10^{-2}

Table 2. Conductivity of Lanthanum doped ceria at various temperatures

Temperature (K)	Conductivity ($mScm^{-1}$)		Activation energy (eV)	
	$Ce_{0.8}La_{0.2}O_2$	$Ce_{0.5}La_{0.5}O_2$	$Ce_{0.8}La_{0.2}O_2$	$Ce_{0.5}La_{0.5}O_2$
873K	0.21	2.36×10^{-2}	0.4	0.3
773K	5.86×10^{-2}	1.59×10^{-2}		
673K	1.39×10^{-2}	1.94×10^{-2}		
573K	1.38×10^{-2}	3.24×10^{-3}		
303K	1.56×10^{-2}	1.95×10^{-2}		

Table 3. Comparison of various conductivity studies with present work

Electrolytes	Temperature	Conductivity (Scm^{-1})	References
$Ce_{0.8}La_{0.2}O_2$	600^0C	0.21×10^{-3}	Present work
$Ce_{0.5}La_{0.5}O_2$	600^0C	2.36×10^{-5}	Present work
$Ce_{0.8}Zr_{0.2}O_2$	1000^0C	8.40×10^{-2}	[48]
$Ce_{0.8}Zr_{0.2}O_{1.9}$	600^0C	0.198×10^{-3}	[49]
$Ce_{0.7}Zr_{0.3}O_{1.85}$	600^0C	0.208×10^{-3}	[49]
$Ce_{0.6}Zr_{0.4}O_{1.8}$	600^0C	0.745×10^{-3}	[49]

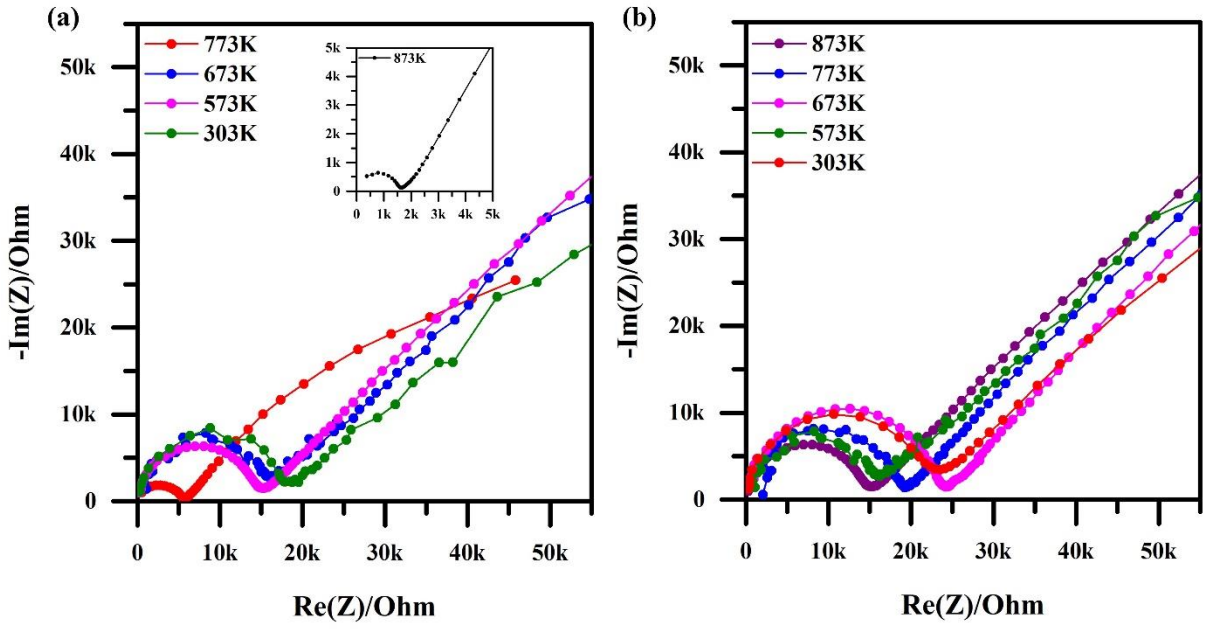

Figure 7. Nyquist plots of LDC electrolyte measured at operating temperatures (a) Ce0.8La0.2O2 (b) Ce0.5La0.5O2 from 303 to 873K

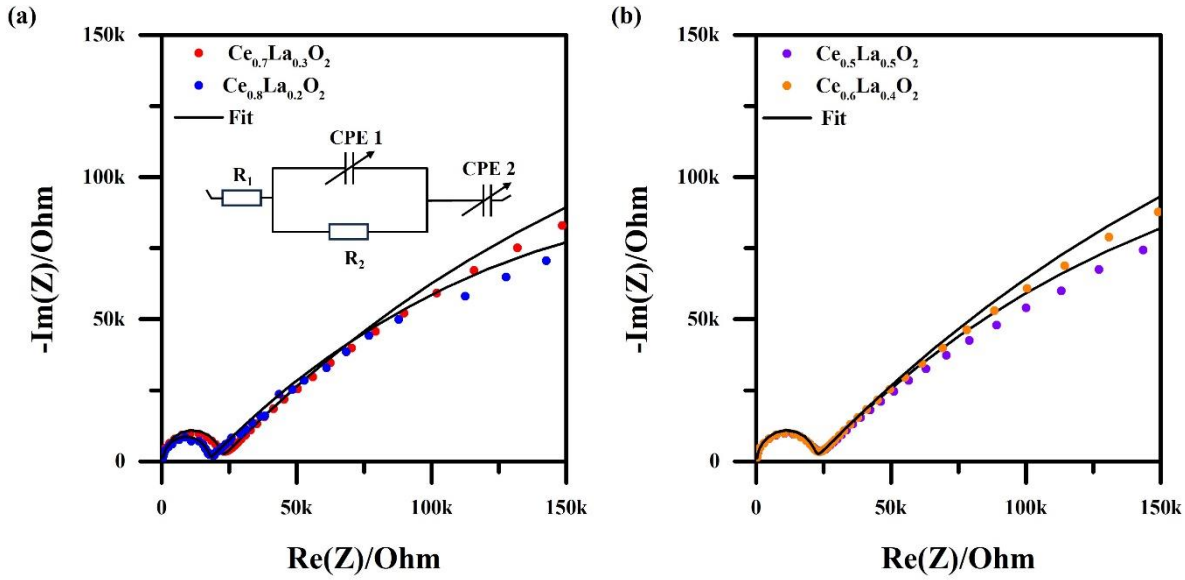

Figure 8. Nyquist plots of LDC electrolyte measured at room temperature (a) $Ce_{0.8}\ La_{0.2}\ O_2$ & $Ce_{0.7}\ La_{0.3}\ O_2$ (b) $Ce_{0.6}\ La_{0.4}\ O_2$ & $Ce_{0.5}\ La_{0.5}\ O_2$

Nyquist plots of $Ce_{0.8}\ La_{0.2}\ O_2$ and $Ce_{0.5}\ La_{0.5}\ O_2$ tested at low temperatures ranging from 873K to 573K shown in figure 8 shows the grain resistance increase as temperature decreases reflected in conductivity values of listed on table 2.

A comparison of various conductivity values with the present study is listed in Table 3. Activation energy Ea was determined by the following relation commonly referred as Arrhenius equation $\sigma = \sigma_0\ e^{-Ea/KT}$. Where (σ) conductivity, (σ_0) pre-exponential factor, (E_a) activation energy, (K) Boltzmann constant, (T) absolute temperature. Thermally activated conduction (Ea activation energy) of $Ce_{0.8}\ La_{0.2}\ O_2$ was determined by plotting log σ (Scm^{-1}) vs $1000/T$ (K^{-1}) and performed a linear fit as shown in figure 9. Activation energy of 0.4 and 0.3 eV was achieved in $Ce_{0.8}La_{0.2}O_2$ and $Ce_{0.5}La_{0.5}O_2$ electrolyte respectively as listed in the Table 2.

On increasing the concentration of La^{3+} ions the activation energy decreases and reaches the lowest value for the composition LDC 0.5 as E_a = 0.3 eV. Even though LDC 0.2 have an higher activation energy of E_a = 0.4 eV it provides an usable conductivity of 0.21 $mScm^{-1}$ at 873K. Electrolytes with low thermal activation energy with reasonable conductivity is high in demand for SOFC applications [49,50].

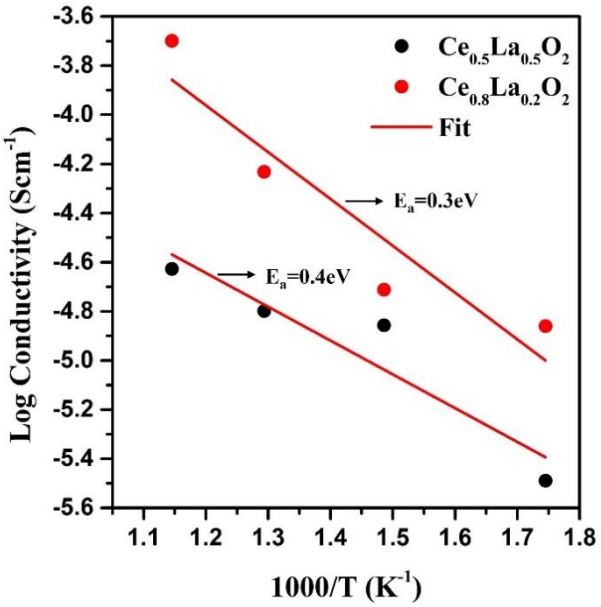

Figure 9. Arrhenius plot of LDC electrolyte measured at operating temperatures from 573 to 873K.

$Ce_{0.8}La_{0.2}O_2$ could be an ideal solid electrolyte for low-temperature SOFC applications with its high conductivity of 0.21 mScm^{-1} at 873K.

4. Conclusion

In this study, La^{3+} ions were successfully incorporated into CeO_2 at La concentrations of x = (0.2, 0.3, 0.4, and 0.5) in $Ce_{1-x}La_xO_{2-\delta}$. XRD analysis confirmed that all samples retained a well-defined cubic fluorite-type structure, with increasing La^{3+} concentrations causing significant peak intensity reduction and broadening and peak splitting indicative of interstitial plane and defect formation within the lattice. Raman spectroscopy supported these findings, showing shifts and intensity changes in the F_{2g} mode, reflecting the impact of La^{3+} doping on the ceria structure. FT-IR spectra revealed subtle changes in the Ce-O vibrational modes, suggesting the structural stability of doped ceria. Optical studies demonstrated consistent UV absorption and a fixed band gap of 3.15 eV across all samples, indicating that the dopant does not alter the lattice but introduces new planes within the CeO_2 crystal. SEM images displayed enhanced interparticle connectivity, larger grain sizes, and a tightly packed surface morphology, which are crucial for various applications, including catalysis and energy storage. EDAX confirmed the presence of cerium and Lanthanum, verifying successful doping. Generally, this study emphasizes the notable impact of La^{3+} doping on the structural, vibrational, and optical properties of CeO_2, emphasizing its potential for enhancing solid electrolyte performance in solid oxide fuel cells and related applications. Conductivity analysis suggests $Ce_{0.8}La_{0.2}O_2$ attained a high conductivity of about 0.21 mScm^{-1} at 873K and a low thermal activation energy of 0.4eV. The findings suggest that La^{3+} doped CeO_2 can be a promising material for advanced energy applications, offering improved structural and functional properties at LT-SOFC applications.

References

[1] X.J. Chen, K.A. Khor, S.H. Chan, L.G. Yu, Influence of microstructure on the ionic conductivity of yttria-stabilized zirconia electrolyte. Materials Science and Engineering: A, 335(1-2), (2002) 246-252. https://doi.org/10.1016/S0921-5093(01)01935-9

[2] A.J. Jacobson, Materials for solid oxide fuel cells. Chemistry of Materials, 22(3) (2010) 660-674. https://doi.org/10.1021/cm902640j

[3] C. Zhang, C.J. Li, G. Zhang, X.J. Ning, C.X. Li, H. Liao, C. Coddet, Ionic conductivity and its temperature dependence of atmospheric plasma-sprayed yttria stabilized zirconia electrolyte. Materials Science and Engineering: B, 137(1-3), (2007) 24-30. https://doi.org/10.1016/j.mseb.2006.10.005

[4] M.D. Mat, X. Liu, Z. Zhu, B. Zhu, Development of cathodes for methanol and ethanol fuelled low temperature (300–600 C) solid oxide fuel cells. International journal of hydrogen energy, 32(7), (2007) 796-801. https://doi.org/10.1016/j.ijhydene.2006.12.012

[5] S.C. Singhal, K. Kendall, (2003) High-temperature solid oxide fuel cells: fundamentals, design and applications. Elsevier.

[6] S. Park, J.M. Vohs, R.J. Gorte, Direct oxidation of hydrocarbons in a solid-oxide fuel cell. Nature, 404(6775), (2000) 265-267.

https://doi.org/10.1038/35005040

[7] Y. Mizutani, M. Tamura, M. Kawai, O. Yamamoto, Development of high-performance electrolyte in SOFC. Solid State Ionics, 72, (1994) 271-275. https://doi.org/10.1016/0167-2738(94)90158-9

[8] H.A. Taroco, J.F. Santos, R.Z. Domingues, T. Matencio, Ceramic materials for solid oxide fuel cells. Advances in ceramics-Synthesis and Characterization, processing and specific applications, (2011) 423-446.

[9] M.C. Brant, T. Matencio, L. Dessemond, R.Z. Domingues, Electrical degradation of porous and dense LSM/YSZ interface. Solid State Ionics, 177(9-10), (2006) 915-921. https://doi.org/10.1016/j.ssi.2006.02.012

[10] C. Varanasi, C. Juneja, C. Chen, B. Kumar, Electrical conductivity enhancement in heterogeneously doped scandia-stabilized zirconia. Journal of power sources, 147(1-2), (2005) 128-135. https://doi.org/10.1016/j.jpowsour.2005.01.028

[11] F. Yuan, J. Wang, H. Miao, C. Guo, W.G. Wang, Investigation of the crystal structure and ionic conductivity in the ternary system (Yb2O3) x–(Sc2O3)(0.11− x)–(ZrO2) 0.89 (x= 0–0.11). Journal of alloys and compounds, 549, (2013) 200-205. https://doi.org/10.1016/j.jallcom.2012.09.089

[12] S. Omar, A. Belda, A. Escardino, N. Bonanos, Ionic conductivity ageing investigation of 1Ce10ScSZ in different partial pressures of oxygen. Solid State Ionics, 184(1), (2011) 2-5. https://doi.org/10.1016/j.ssi.2010.09.042

[13] M. Hirano, T. Oda, K. Ukai, Y. Mizutani, Effect of Bi2O3 additives in Sc stabilized zirconia electrolyte on a stability of crystal phase and electrolyte properties. Solid State Ionics, 158(3-4), (2003) 215-223. https://doi.org/10.1016/S0167-2738(02)00912-8

[14] Y. Arachi, T. Asai, O. Yamamoto, Y. Takeda, N. Imanishi, K. Kawate, C. Tamakoshi, Electrical conductivity of ZrO2 Sc2O3 doped with HfO2, CeO2, and Ga2O3. Journal of the Electrochemical Society, 148(5), (2001) A520. https://doi.org/10.1149/1.1366622

[15] Z. Lei, Q. Zhu, Phase transformation and low temperature sintering of manganese oxide and scandia co-doped zirconia. Materials letters, 61(6), (2007) 1311-1314. https://doi.org/10.1016/j.matlet.2006.07.020

[16] A.S. Nesaraj, (2010) Recent developments in solid oxide fuel cell technology–a review. CSIR, 169-176.

[17] B. Zhu, Functional ceria–salt-composite materials for advanced ITSOFC applications. Journal of Power sources, 114(1), (2003) 1-9. https://doi.org/10.1016/S0378-7753(02)00592-X

[18] M. Dudek, Composite oxide electrolytes for electrochemical devices. Advances in Materials Science, 8(1), (2008) 15-30. https://doi.org/10.2478/v10077-008-0002-9

[19] S. Kuharuangrong, Ionic conductivity of Sm, Gd, Dy and Er-doped ceria. Journal of Power Sources, 171(2), (2007) 506-510. https://doi.org/10.1016/j.jpowsour.2007.05.104

[20] M.L. Faro, D. La Rosa, V. Antonucci, A.S. Arico, Intermediate temperature solid oxide fuel cell electrolytes. Journal of the Indian Institute of Science, 89(4), (2009) 363-380.

[21] H. Inaba, H. Tagawa, Ceria-based solid electrolytes. Solid state ionics, 83(1-2), (1996) 1-16. https://doi.org/10.1016/0167-2738(95)00229-4

[22] A. Gondolini, E. Mercadelli, A. Sanson, S. Albonetti, L. Doubova, S. Boldrini, Microwave-assisted synthesis of gadolinia-doped ceria powders for solid oxide fuel cells. Ceramics International, 37(4), (2011) 1423-1426. https://doi.org/10.1016/j.ceramint.2011.01.010

[23] J.W. Fergus, Electrolytes for solid oxide fuel cells. Journal of power sources, 162(1), (2006) 30-40. https://doi.org/10.1016/j.jpowsour.2006.06.062

[24] M. Dudek, Ceramic electrolytes in the CeO2-Gd2O3-SrO system-Preparation, properties and application for solid oxide fuel cells. International Journal of Electrochemical Science, 7(4), (2012) 2874-2889. https://doi.org/10.1016/S1452-3981(23)13921-6

[25] J. Fergus, R. Hui, X. Li, D.P. Wilkinson, J. Zhang, (2016) Solid oxide fuel cells: materials properties and performance. CRC press. https://doi.org/10.1201/9781420088847

[26] B. Li, X. Wei, W. Pan, Improved electrical conductivity of Ce0.9Gd0.1O1.95 and Ce0.9Sm0.1O1.95 by co-doping. International journal of hydrogen energy, 35(7), (2010) 3018-3022. https://doi.org/10.1016/j.ijhydene.2009.07.002

[27] Y. Zheng, Y. Shi, H. Gu, L. Gao, H. Chen, L. Guo, La and Ca co-doped ceria-based electrolyte materials for IT-SOFCs. Materials Research Bulletin, 44(8), (2009) 1717-1721. https://doi.org/10.1016/j.materresbull.2009.03.017

[28] A. Rafique, R. Raza, N. Akram, M.K. Ullah, A. Ali, M. Irshad, K. Siraj, M. Ajmal Khan, B. Zhu, R. Dawson, Significance enhancement in the conductivity of core shell nanocomposite electrolytes. RSC advances, 5(105), (2015) 86322-86329. https://doi.org/10.1039/C5RA16763A

[29] M. Kahlaoui, S. Chefi, A. Inoubli, A. Madani, C. Chefi, Synthesis and electrical properties of co-doping with La3+, Nd3+, Y3+, and Eu3+ citric acid-nitrate prepared samarium-doped ceria

ceramics. Ceramics International, 39(4), (2013) 3873-3879. https://doi.org/10.1016/j.ceramint.2012.10.230

[30] Y.P. Fu, S.B. Wen, C.H. Lu, Preparation and characterization of samaria-doped ceria electrolyte materials for solid oxide fuel cells. Journal of the American Ceramic Society, 91(1), (2008) 127-131. https://doi.org/10.1111/j.1551-2916.2007.01923.x

[31] N. Jaiswal, S. Upadhyay, D. Kumar, O. Parkash, Ionic conductivity investigation in lanthanum (La) and strontium (Sr) co-doped ceria system. Journal of power sources, 222, (2013) 230-236. https://doi.org/10.1016/j.jpowsour.2012.08.095

[32] Dudek, M. (2008). Ceramic oxide electrolytes based on CeO2—preparation, properties and possibility of application to electrochemical devices. Journal of the European ceramic society, 28(5), 965-971. https://doi.org/10.1016/j.jeurceramsoc.2007.09.004

[33] N. Mahato, A. Banerjee, A. Gupta, S. Omar, K. Balani, Progress in material selection for solid oxide fuel cell technology: A review. Progress in Materials Science, 72, (2015) 141-337. https://doi.org/10.1016/j.pmatsci.2015.01.001

[34] H. Hayashi, M. Kanoh, C.J. Quan, H. Inaba, S. Wang, M. Dokiya, H. Tagawa, Thermal expansion of Gd-doped ceria and reduced ceria. Solid State Ionics, 132(3-4), (2000) 227-233. https://doi.org/10.1016/S0167-2738(00)00646-9

[35] L. Zhang, M. Liu, J. Huang, Z. Song, Y. Fu, Y. Chang, C. Li, T. He, (2014) Improved thermal expansion and electrochemical performances Ba0.6Sr0.4Co0.9Nb0.1O3−δ–Gd0.1Ce0.9O1.95 composite cathodes for IT-SOFCs. International journal of hydrogen energy, 39(15), 7972-7979. https://doi.org/10.1016/j.ijhydene.2014.03.055

[36] K. Venkataramana, C. Madhusudan, C. Madhuri, C.V. Reddy, Synthesis, characterization and thermal expansion of Ce0. 8–xSm0. 2ZrxO2-δ Solid electrolytes for IT-SOFC applications. Materials Today: Proceedings, 3(10), (2016) 3908-3913. https://doi.org/10.1016/j.matpr.2016.11.048

[37] A. Ali, R. Raza, M. Kaleem Ullah, A. Rafique, B. Wang, B. Zhu, Alkaline earth metal and samarium co-doped ceria as efficient electrolytes. Applied Physics Letters, 112(4), (2018). https://doi.org/10.1063/1.5005824

[38] N. Momin, J. Manjanna, Ionic Conductivity of Ce0. 91Ca0. 09O2-d as an Electrolyte for Intermediate Temperature Solid Oxide Fuel Cells. Research Journal of Chemistry and Environment, 25(1), (2021) 1-9. https://doi.org/10.25303/2512rjce001009

[39] N. Jaiswal, D. Kumar, S.Upadhyay, O. Parkash, Ceria co-doped with calcium (Ca) and strontium (Sr): a potential candidate as a solid electrolyte for intermediate temperature solid oxide fuel cells. Ionics, 20, (2014) 45-54. https://doi.org/10.1007/s11581-013-0936-8

[40] N. Momin, J. Manjanna, S. Kobayashi, S.T. Aruna, S.S. Kumar, G.P. Nayaka, Synthesis and ionic conductivity of calcium-doped ceria relevant to solid oxide fuel cell applications. Materials Advances, 3(23), (2022) 8780-8791. https://doi.org/10.1039/D2MA00868H

[41] N. Momin, J. Manjanna, L. D'Souza, S.T. Aruna, S.S. Kumar, Synthesis, structure and ionic conductivity of nanocrystalline Ce1− xLaxO2− δ as an electrolyte for intermediate temperature solid oxide fuel cells. Journal of Alloys and Compounds, 896, (2022)163012. https://doi.org/10.1016/j.jallcom.2021.163012

[42] J. Zdravkovic, B. Simovic, A. Golubovic, D. Poleti, I. Veljkovic, M. Scepanovic, G. Brankovic, Comparative study of CeO2 nanopowders obtained by the hydrothermal method from various precursors. Ceramics International, 41(2), (2015) 1970-1979. https://doi.org/10.1016/j.ceramint.2014.08.122

[43] T. Jeyakumaran, N. Venkatesh Bharathi, R. Shanmugavel, P. Sriramachandran, S. Ramaswamy, Structural, Vibrational, Optical and Improved Photoluminescence Properties of Dy 3+ Doped $Ca_2KZn_2V_3O_{12}$ Phosphors. Journal of Inorganic and Organometallic Polymers and Materials, 31, (2021) 695-703. https://doi.org/10.1007/s10904-020-01766-5

[44] W.H. Weber, K.C. Hass, J.R. McBride, Raman study of CeO2: Second-order scattering, lattice dynamics, and particle-size effects. Physical Review B, 48(1), (1993) 178. https://doi.org/10.1103/PhysRevB.48.178

[45] O. Kraynis, I. Lubomirsky, T. Livneh, Resonant Raman scattering in undoped and lanthanide-doped CeO2. The Journal of Physical Chemistry C, 123(39), (2019) 24111-24117. https://doi.org/10.1021/acs.jpcc.9b06918

[46] J. Liu, Z. Zhao, Y. Chen, C. Xu, A. Duan, G. Jiang, Different valent ions-doped cerium oxides and their catalytic performances for soot oxidation. Catalysis today, 175(1), (2011) 117-123. https://doi.org/10.1016/j.cattod.2011.05.023

[47] A. Kalpana Devi, G. Ram Kumar, C. Prerna, K. Amarsingh Bhabu, V. Sabarinathan, T.R. Rajasekaran, Superionic conductive La 3+ and Pr 3+ Co-doped cerium oxide for IT-SOFC applications. Journal of Materials Science: Materials in Electronics, 31, (2020) 10628-10638. https://doi.org/10.1007/s10854-020-03612-3

[48] M. Boaro, S. Desinan, C. Abate, M. Ferluga, C. de Leitenburg, A. Trovarelli, Study on Redox, Structural and Electrical Properties of Ce x Zr1− x O2 for Applications in SOFC Anodes. Journal of the Electrochemical Society, 158(2), (2010) 22.

https://doi.org/10.1149/1.3518756

[49] K.A. Bhabu, J. Theerthagiri, J. Madhavan, T. Balu, G. Muralidharan, T.R. Rajasekaran, Enhanced electrochemical behavior of ceria based zirconia electrolytes for intermediate temperature solid oxide fuel cell applications. Journal of Materials Science: Materials in Electronics, 27, (2016) 10980-10992. https://doi.org/10.1007/s10854-016-5214-x

[50] A. Lakshmanan, S. Venkatachalam, Effect Temperature for improving the Li-ion conductivity of Li7La3Zr2O12. International Research Journal of Multidisciplinary Technovation, 6(1), (2024) 82-96. https://doi.org/10.54392/irjmt2417

Authors Contribution Statement

S. Seema – Conceptualization, Invegtiation, data collection, Fomal Anlysis and Writing - original draft. **T. Thangesh** - Data collection. **V. Sabarinathan** - Supervision, Writing – review & editing. **T. R. Rajasekaran** - Conceptualization, Writing – review & editing. **S. Nagarajan** - Writing – review & editing. All the author's read and approved the final version of the manuscript.

Acknowledgement

S. Seema thanks the Rashtriya Uchchatar Shiksha Abhiyan (RUSA), Government of India, for providing the characterization facilities at the Department of Renewable Energy Science, Manonmaniam Sundaranar University, Tirunelveli, Tamilnadu, India.

Funding

The authors declare that no funds, grants or any other support were received during the preparation of this manuscript.

Competing Interests

The authors declare that there are no conflicts of interest regarding the publication of this manuscript.

Data Availability

The data supporting the findings of this study can be obtained from the corresponding author upon reasonable request.

Has this article screened for similarity?

Yes

About the License